Environmental Science & Technology

pubs.acs.org/est

Article

Development and Assessment of a High-Resolution Biogenic Emission Inventory from Urban Green Spaces in China

Mingchen Ma, Yang Gao,* Aijun Ding, Hang Su, Hong Liao, Shuxiao Wang, Xuemei Wang, Bin Zhao, Shaoqing Zhang, Pingqing Fu, Alex B. Guenther, Minghuai Wang, Shenshen Li, Biwu Chu, Xiaohong Yao, and Huiwang Gao

Cite This: *Environ. Sci. Technol.* 2022, 56, 175−184

Read Online

ACCESS | Metrics & More | Article Recommendations | Supporting Information

ABSTRACT: Biogenic volatile organic compound (BVOC) emissions have long been known to play vital roles in modulating the formation of ozone and secondary organic aerosols (SOAs). While early studies have evaluated their impact globally or regionally, the BVOC emissions emitted from urban green spaces (denoted as U-BVOC emissions) have been largely ignored primarily due to the failure of low-resolution land cover in resolving such processes, but also because their important contribution to urban BVOCs was previously unrecognized. In this study, by utilizing a recently released high-resolution land cover dataset, we develop the first set of emission inventories of U-BVOCs in China at spatial resolutions as high as 1 km. This new dataset resolved densely distributed U-BVOCs in urban core areas. The U-BVOC emissions in megacities could account for a large fraction of total BVOC emissions, and the good agreement of the interannual variations between the U-BVOC emissions and ozone concentrations over certain regions stresses their potentially crucial role in influencing ozone variations. The newly constructed U-BVOC emission inventory is expected to provide an improved dataset to enable the research community to re-examine the modulation of BVOCs on the formation of ozone, SOA, and atmospheric chemistry in urban environments.

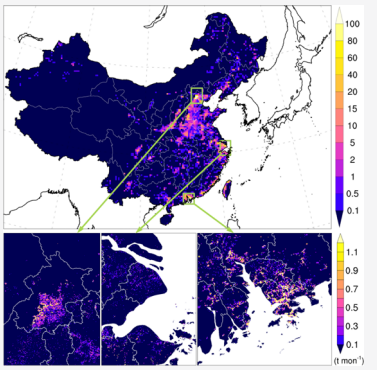

KEYWORDS: *biogenic emissions, ozone, urban green spaces, U-BVOC emissions*

1. INTRODUCTION

Biogenic volatile organic compound (BVOC) emissions are defined as volatile and semi-volatile organic chemical species that are emitted by terrestrial ecosystems, including plants, soils, earth activities, and so forth,[1] and are widely regarded as the most important source of volatile organic compounds (VOCs) in the world and are 1 order of magnitude higher than anthropogenic sources.[2] BVOCs play important roles in elevating the formation of both ozone[3−6] and secondary organic aerosols (SOAs).[7−9]

Although it has been estimated that 90% of global BVOCs are emitted by vegetation,[10] previous studies have widely examined the BVOC emissions from the natural environment[11] and the emissions from the vegetation from urban areas are to a large extent either underestimated or ignored.[6,12−14] The primary reason lies in the difficulty in characterizing urban vegetation when the relatively coarse spatial resolutions of land cover data are applied.[15] The spatial resolution of the widely adopted land cover data, that is, with a moderate resolution imaging spectroradiometer (MODIS) MCD12Q1,[16] is normally a few hundred meters, which is unable to resolve urban green spaces.

Although the urban vegetation densities are much smaller than those in natural forests, the urban BVOC emission intensities could be larger than those in natural environments. This is primarily due to the higher temperatures due to the urban heat island effect,[17,18] more solar radiation because of open canopies,[19] greater plant biomass,[20] as well as artificially selected species with higher emission factors.[21] For instance, Chang et al.[22] discovered that the annual averaged BVOC emission intensities in an urban green space (3.13 t C km^{-2} yr^{-1}) were larger than those in rural forests (2.74 t C km^{-2} yr^{-1}) in Hangzhou, China, based on field measurements of vegetation biomass, species, and emission rates. Not only are the intensities high, the total amounts of BVOC emissions are also nontrivial. For instance, the BVOC emissions from the urban landscape accounted for 15% of the total BVOC emissions in Beijing, China, in 2015, as was determined by incorporating vegetation surveys.[23]

Moreover, the BVOC emissions in urban areas play critical roles in urban air quality[24] and tend to be more efficient in triggering ozone enhancement.[25] For example, the same

Received: September 15, 2021
Revised: November 22, 2021
Accepted: December 1, 2021
Published: December 13, 2021

percentage increase in BVOC emissions in urban areas may foster twice the ozone increase as that over rural areas.[25,26] The addition of urban BVOC emissions may substantially increase the simulated ozone precursors such as isoprene concentrations.[15] Moreover, it is widely acknowledged that underestimations in the simulated ozone concentrations exist during ozone episodes, particularly when the ozone concentrations are extremely high (e.g., Sun et al.,[27] Wang et al.,[28] Lu et al.,[29] and Ma et al.[15]), which could be reduced dramatically through the implementation of improved estimates of the emissions of ozone precursors.

Artificial impervious areas indicative of urbanized areas have increased rapidly in the past 30 years, especially in China, which has become the country with the largest amount of artificial impervious areas in the world since 2015.[30] Meanwhile, there has been an increase in urban green space coverage. For instance, the mean coverage of urban green spaces in 286 cities of China increased from 17.0% in 1989 to 37.3% in 2009,[31] and the total areas of urban green spaces in China have increased by 83% from 2000 (1.00×10^4 km^2) to 2018 (1.83×10^4 km^2) due to urban expansion and increased urban greening.[32] Therefore, it is of great importance to develop an emission inventory of BVOCs over the urban areas in China, which should shed light on relevant studies in the rest of the world.

By taking advantage of the global land cover dataset with a high spatial resolution of 10 m (FROM-GLC10),[33] an urban BVOC emission inventory in China has been, to our knowledge, for the first time developed and evaluated at a multi-year scale from 2015 to 2019. In addition, a comparison with the traditionally used MODIS data at 500 m resolution was also conducted.

2. METHODS

2.1. Model Configurations. The biogenic emission model, Model of Emissions of Gases and Aerosols from Nature version 2.1 (MEGANv2.1[10,34]), is applied to estimate BVOC emissions. In MEGANv2.1, more than 150 VOCs from terrestrial ecosystems are included and classified into 18 categories. The emission rate F_i (μg m^{-2} h^{-1}) of each VOC category (denoted as i) is calculated, as shown in eq 1

$$F_i = \gamma_i \sum \varepsilon_{i,j} \chi_j \quad (1)$$

$$\gamma_i = C_{CE} \cdot \gamma_{L,i} \gamma_{T,i} \gamma_{LA,i} \gamma_{SM,i} \gamma_{CI,i} \cdot \mathrm{LAI} \quad (2)$$

where ε represents the emission factor (EF) of each VOC category i and plant functional type (PFT) j and is denoted as $\varepsilon_{i,j}$ and χ_j that represent the fraction of each PFT. γ_i is an emission activity factor, which is calculated by eq 2. C_{CE} represents the canopy environmental factor, for which a default value of 0.57 in MEGAN is used here. $\gamma_{*,i}$ is an environmental factor, where the symbol asterisk (*) can be replaced by light (L), temperature (T), leaf age (LA), soil moisture (SM), or CO_2 inhabitation (CI). LAI is the leaf area index.

The meteorological parameters used in eq 1 were provided by simulations from the Weather Research and Forecasting (WRF) model v3.8.1, and the physics options used are consistent with those used in our previous studies.[35−38] A total of four domains are designed with horizontal resolutions of 27, 9, 3, and 1 km (Figure 1), with at least 5 grids in the boundaries between the nest and mother domain, as previously described.[39] Grid nudging is applied only to horizonal winds above the planetary boundary layer in the outer domain (27 km), with a nudging coefficient of 0.0003 s^{-1}.[40] The simulations at the spatial resolution of 27 km are conducted over the five-year period from 2015 to 2019, while for the other resolutions (9, 3, and 1 km), the simulations are from June to August in 2017, considering the limitations of computational resources. One-way nested runs are conducted from 27 to 1 km, with one nested simulation from 27 to 9 km, followed by three nested runs at spatial resolutions of 3 and 1 km over the North China Plain (NCP), Yangtze River Delta (YRD), and Pearl River Delta (PRD), respectively. The initial and boundary conditions for the outer domain (at spatial resolution of 27 km) is from the NCEP Climate Forecast System Reanalysis (CFSR) version 2,[41] with a spatial resolution of 0.5°. The selected meteorological parameters associated with MEGAN are evaluated (Supporting Information Table 1) and show reasonable performance compared to the observations available at the National Climatic Data Center (NCDC; https://www.ncdc.noaa.gov/cdo-web/, last access: 14 November 2021). A total of 34 vertical layers are selected with a model top of 50 hPa.

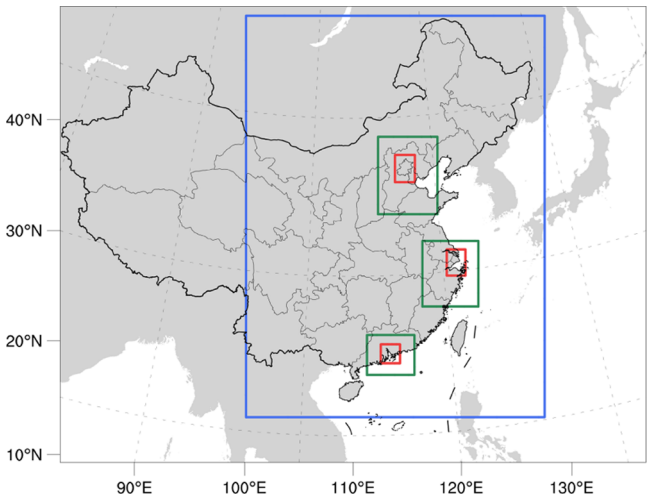

Figure 1. Simulation domains with grid spacings of 27 km (outer domain), 9 km (blue), 3 km (green), and 1 km (red).

2.2. PFTs, LAIs, and EFs Used in This Study. The EFs (ε) vary with each PFT, and the widely used ones are those that are obtained directly from the look-up table (Table 2 in Guenther et al.[34]), including factors for 16 types of PFTs (referred to as 16-PFT thereafter, as shown in Supporting Information Table 2), which shows that the differences in EFs among different PFTs are quite large. For instance, the isoprene emission factor for broadleaf deciduous boreal trees is 11 000 μg m^{-2} h^{-1} but it is only 1 μg m^{-2} h^{-1} for needleleaf deciduous boreal trees. To use the look-up table, the available land cover datasets need to match the 16-PFT data.

In this study, two land cover datasets are selected to estimate the BVOC emissions from urban green spaces, which are defined as U-BVOC emissions, including MODIS MCD12Q1[16] at a spatial resolution of 500 m and a dataset with a higher spatial resolution of 10 m, FROM-GLC10.[33] Considering that the FROM-GLC10 data is available only in the year of 2017, the same year of MODIS data is used to keep consistency. There are a total of eight vegetation types in MODIS (Supporting Information Table 3), and the method to match them to the 16-PFT data has been fully discussed in the

https://doi.org/10.1021/acs.est.1c06170
Environ. Sci. Technol. 2022, 56, 175−184

Table 1. Comparison of Emissions between This Study[a] and Previous Studies (Unit: Tg yr^{-1})

	year	T-BVOCs[b]	isoprene	terpenes	OVOCs
MODIS	2015−2019	29.28 ± 0.91	13.88 ± 0.57	5.28 ± 0.12	10.13 ± 0.21
FROM-GLC10	2015−2019	31.42 ± 0.95	14.29 ± 0.54	4.77 ± 0.11	12.36 ± 0.30
Guenther et al.[2]	1990	28.4	15.0	4.3	9.1
Klinger et al.[46]	2000	20.6	4.1	3.5	13.0
Chi and Xie[47]	2003	12.83	7.45	2.23	3.14
Li et al.[48]	2003	42.5	20.7	4.9	13.5
Wu et al.[45]	2017	23.54	13.30	3.09	7.15

[a]The values in the first two rows are the results of this study, indicating emissions from the MODIS and FROM-GLC10 data, respectively. [b]The emissions of T-BVOCs (T-BVOC emissions; third column) are equivalent to the summation of emissions of isoprene, terpenes, and OVOCs (columns four to six).

Methods section as well as in Table S4 in Ma et al.[15] In contrast, only four vegetation types (e.g., "forest", "grass", "shrub", and "crop"; Supporting Information Table 4) are available in the FROM-GLC10 dataset; so they are first allocated to match those in MODIS and are followed by a repetitive conversion procedure to the 16-PFT data, as mentioned above. Considering that "grass", "shrub", and "crop" are common between the MODIS and FROM-GLC10 data, only "forest" needs to be allocated, which is detailed below.

There are two cases in total. First, for any grid classified as "forest" in the FROM-GLC10 data, when the corresponding MODIS grid (based on the longitude/latitude coordinates) is trees (e.g., including needle evergreen trees, needle deciduous trees, broadleaf evergreen trees, and broadleaf deciduous trees; Supporting Information Table 3), the FROM-GLC10 pixel point is allocated to the same tree type as that in the MODIS data. Second, for any grid that is classified as "forest" in the FROM-GLC10 data, the corresponding grid in the MODIS data is not trees, and the grid type in the FROM-GLG10 data is assigned to "broadleaf trees", which is the most widely distributed tree type in the study area (Figure 1; e.g., the areas of "broadleaf trees" account for 67% of all the types of "trees" in the outer domain based on MODIS). This broadleaf tree type is further assigned to either broadleaf deciduous trees or broadleaf evergreen trees based on the latitude.

The monthly LAIs in MODIS are based on the averages of the 8 day MODIS MCD15A2H,[42] whereas for the FROM-GLC10 data, the derivation of LAI over each grid at 10 m is calculated based on the existing PFT data as well as the empirical relationship between PFTs and LAIs provided in Zhang et al.[43] Nevertheless, it is admitted that there are uncertainties associated with the method due to the lack of accounting for spatial heterogeneity in the empirical relationship mentioned above, and further improvement in a high resolution LAI data set is desired in future.

The resulting PFTs, LAIs, and EFs associated with MODIS and FROM-GLC10, summarized in Supporting Information Table 5, are used in MEGAN to calculate the total BVOC (denoted as T-BVOC) emissions, including the emissions of isoprene, terpenes (a total of 73 compounds), and other VOCs that contains 77 compounds such as hexenol, methanol, acetone, and methane (denoted as OVOCs).

2.3. Identification of Urban Green Spaces and U-BVOC Emissions. To identify the U-BVOC emissions, the first challenge is to identify the urban core areas that are demarcated by urban boundaries. The urban core area is defined, based on MODIS, as consisting of those grids with a land cover type of "urban and built-up lands", where no BVOC emissions exist, which is indicative of zero U-BVOC emissions from the MODIS data. In this context, the T-BVOC emissions generated from the land cover in the MODIS data are equivalent to the BVOC emissions from a non-urban environment (denoted as N-BVOC emissions). The above-defined urban core area is further projected to FROM-GLC10, and the BVOC emissions that result from the land cover in the FROM-GLC10 data are classified as U-BVOC emissions. The result of subtracting the U-BVOC emissions from the T-BVOC emissions based on the FROM-GLC10 data is equal to the N-BVOC emissions, which is comparable in magnitude to that based on the MODIS data. Therefore, the terms U-BVOC and N-BVOC emissions hereafter indicate the emissions determined from the FROM-GLC10 and MODIS data, respectively.

2.4. Ozone Formation Potential. To investigate the potential impact of BVOC emissions on ozone formation, the ozone formation potential (OFP) of emissions of each BVOC species k is calculated from eq 3. It is noteworthy that the OFP is an emission-based indicator, and the effect of other factors (e.g., meteorology) on ozone formation could be quantified by air quality models.

$$\mathrm{OFP_k} = E_k \times \mathrm{MIR_k} \quad (3)$$

where $\mathrm{OFP_k}$ represents the OFP of each species (g O_3/year), E_k represents the emission rate (g $\mathrm{BVOC_k}$/year) of BVOC species k, and $\mathrm{MIR_k}$ (g O_3/g $\mathrm{BVOC_k}$) represents the maximal incremental reactivity of the corresponding BVOC species k.[44]

3. RESULTS

3.1. T-BVOC Emissions in China from 2015 to -2019. Based on the MODIS and FROM-GLC10 land cover datasets, the T-BVOC emissions in China from 2015 to 2019 are estimated to be comparable, namely, 29.28 ± 0.91 and 31.42 ± 0.95 Tg yr^{-1}, respectively. The emissions are dominated by isoprene emissions, which account for nearly half of the T-BVOC emissions. The slightly higher T-BVOC emissions based on the FORM-GLC10 data than the MODIS data are primarily a result of more crops and thus a higher amount of OVOCs. In terms of the spatial distributions (Supporting Information Figure 1), while a comparable pattern is achievable between the two datasets, it is obvious that higher T-BVOC emissions based on the FROM-GLC10 data are found along a northeast-southwest belt centered around Beijing, which are due to the identification of a larger amounts of trees in the FROM-GLC10 data compared to the MODIS data (Supporting Information Figures 2 and 3). Interestingly, this belt coincides with areas rich in BVOCs in northern China, which further stress the potentially more important role

https://doi.org/10.1021/acs.est.1c06170
Environ. Sci. Technol. 2022, 56, 175−184

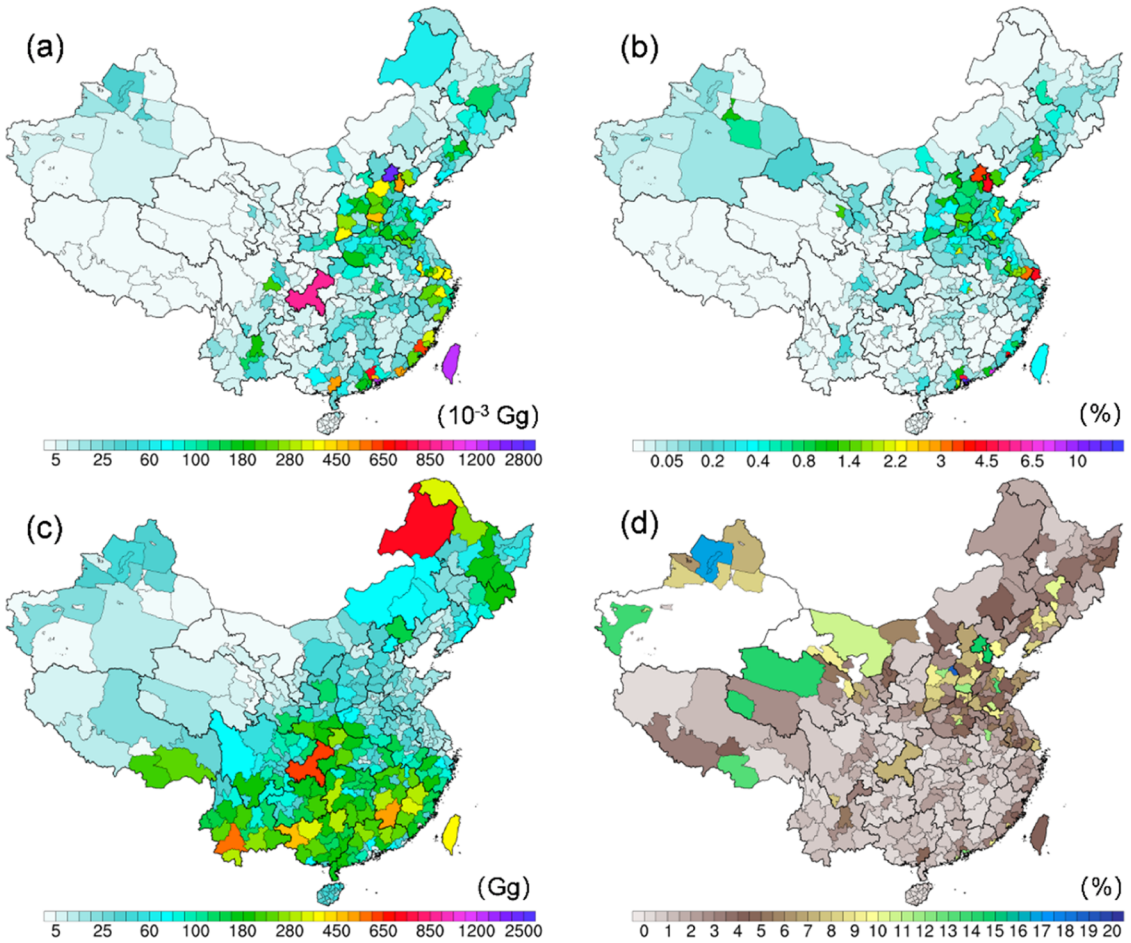

Figure 2. Spatial distributions of annual U-BVOC (a) and N-BVOC (c) emissions, ratios of U-BVOC to N-BVOC emissions (b), and ratios of the U-BVOC to N-BVOC emission intensities (d) at the city level averaged from 2015 to 2019.

of BVOCs in these areas for model simulations that replace the traditionally used MODIS data.

Compared with the T-BVOC emissions reported in previous studies (Table 1), our results are generally within their ranges. In particular, when compared to a recent study by Wu et al.,[45] while comparable amounts of T-BVOC emissions are estimated, the slightly higher OVOC emissions reported by our study are attributable to the modifications of the default EFs based on the look-up table from Table 2 in Guenther et al.[34] The default EF datasets used by Wu et al.[45] consisted of gridded data with a spatial resolution of 1 km by 1 km globally from the standard MEGAN input from the website (https://bai.ess.uci.edu/megan; last access: 30 August 2021), which only considered a limited group of OVOCs and led to lower OVOC emissions. The BVOC emissions from the previous studies exhibited large differences, possibly resulting from different land cover datasets, emission factors, emission calculation algorithms, and meteorological conditions.

As was discussed in the Methods section, the FROM-GLC10 data include urban green spaces, which indicates that U-BVOC emissions are included. Considering the missing U-BVOC emissions in the previous study, it is useful to focus on these U-BVOC emissions and conduct a thorough evaluation.

3.2. Estimation of U-BVOC Emissions. Based on the method discussed in Section 2.3, the total corresponding urban green spaces are 26 641 km^2 in China, which is ~18% higher than the value (22 635 km^2) calculated based on the 2017 China City Statistical Yearbook (http://www.stats.gov.cn/; last access: 16 November 2021) and is ~46% higher than that (1.83×10^4 km^2) in 2018 based on Landsat images with a spatial resolution of 30 m.[32]

The annual U-BVOC emissions in China that were averaged from 2015 to 2019 are 28.91 ± 0.89 Gg yr^{-1}, which include 8.59 ± 0.28 Gg yr^{-1} of isoprene, 1.87 ± 0.03Gg yr^{-1} of terpenes, and 18.46 ± 0.58 Gg yr^{-1} of OVOCs. The U-BVOC emissions account for 0.1% of the T-BVOC emissions (Table 1) in China, and the emissions at the provincial level are shown in Supporting Information Table 6. Most areas with high U-BVOC emissions are located in the developed part of central-eastern China. For instance, the province with the highest U-BVOC emissions, as well as for individual species such as isoprene and terpenes, is Guangdong (4.69 Gg yr^{-1}), where ozone pollution is a substantial concern.[49,50] This is followed by Beijing (2.88 Gg yr^{-1}) which often faces severe ozone problems.[51,52] The U-BVOC emissions in Beijing account for 62% of those in Guangdong, although its area is only about 10% (with area percentage calculation based on the borderline of provinces), and the ratio difference is primarily attributable to the larger fraction in the area of urban trees in Beijing. Similarly, the U-BVOC emissions in Hong Kong is 23% of those in Guangdong, while its area is less than 1% that of Guangdong. Moreover, the U-BVOC emissions in Beijing estimated in our study are only approximately half of the amount estimated in Ren et al.[23] The primary reasons are the

https://doi.org/10.1021/acs.est.1c06170
Environ. Sci. Technol. 2022, 56, 175−184

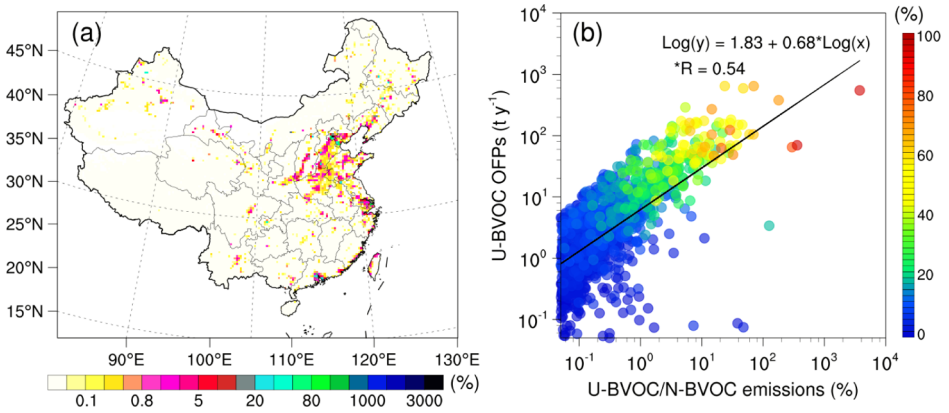

Figure 3. Spatial distribution of the ratio of U-BVOC to N-BVOC emissions (a) and the log−log relationship between the U-BVOC OFPs and ratios of U-BVOC to N-BVOC emissions (b) (the colors of the dots represent the urban area percentages in each grid). The 5 yr data from 2015 to 2019 were applied with the average values used for each grid or dot.

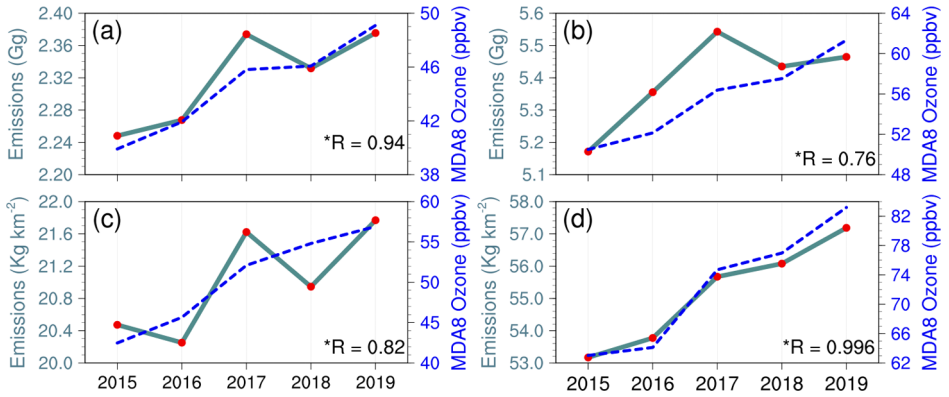

Figure 4. Inter-annual variations in U-BVOC emissions and MDA8 ozone levels on the annual (left) and summer (right) basis over China (top) and NCP (bottom); all the units of the emissions displayed on the left *y*-axis are scaled to the monthly total. The asterisk on the top left of *R* indicates statistical significance ($P < 0.05$).

larger area of urban trees in Beijing described in their study (351 km^2) when compared to our estimate based on the FROM-GLC10 data (174 km^2), as well as the larger emission factors used in their study (e.g., Tables S5 and S6 in the Supporting Information in Ren et al.[23]). In addition, the ratios of the U-BVOC emissions (from FROM-GLC10) to the N-BVOC emissions (from MODIS) at the provincial level are shown in Supporting Information Figure 4, which show that the high ratios are mainly located in northern China, such as Hebei Province and Shandong Province.

Despite the small fraction in terms of the provincial scale contributions, the characteristics of the urban green space distributions may lead to larger ratios or fractions at the city level. Therefore, the spatial distributions of the U-BVOC emissions, N-BVOC emissions, as well as the ratios of the U-BVOC to N-BVOC emissions at the city-level are shown in Figure 2. The distributions of the U-BVOC emissions are spatially heterogeneous, and the areas with larger ratios of U-BVOC to N-BVOC emissions are mainly located in well-developed regions that are also ozone-pollution-prone regions, which include the NCP, YRD, and PRD. For instance, the U-BVOC emissions in Beijing (over the NCP), Shanghai (over the YRD), and Hong Kong (over the PRD) are 2.88, 0.35, and 1.06 Gg yr^{-1} (Figure 2a), respectively, which account for 3.4, 4.6, and 11.7% (Figure 2b) relative to N-BVOC emissions, respectively. Please note that the U-BOVC emissions in Chongqing (shown in magenta in southwestern China in Figure 2a) are 0.85 Gg, which rank among the top five cities considering the large amount of urban green spaces; nevertheless, the fraction relative to the N-BVOC emissions is 0.1% (Figure 2c) due to large N-BVOC emissions therein. These regions are often rich in NOx and are located in VOC-limited regimes.[5] The U-BVOCs such as isoprene are reported to trigger ozone formation approximately twice as efficiently as that from N-BVOCs in a megacity like Beijing based on a numerical study conducted in early summer 2017.[25] Over these VOC-limited areas, the inclusion of U-BVOC emissions may substantially foster the ozone enhancement.[15]

To make further comparisons between the U-BVOC and N-BVOC emissions, their ratios over each grid at a spatial resolution of 27 km by 27 km averaged from 2015 to 2019 are shown in Figure 3a and exhibit larger contributions of U-BVOCs relative those at the city-level depicted in Figure 2. For example, the ratios of the U-BVOC to N-BVOC emissions over some locations in megacities such as Beijing and Shanghai may reach 100% or more. This result indicates that while there are generally smaller magnitudes of U-BVOC emissions compared to N-BVOC emissions, there are areas with U-BVOC emission levels that even exceed the amounts of N-BVOC emissions, which are indicative of the potentially important role of U-BVOCs in affecting the urban atmospheric chemistry such as ozone and SOA formation in these air pollution-prone regions.

https://doi.org/10.1021/acs.est.1c06170
Environ. Sci. Technol. 2022, 56, 175−184

The impacts of U-BVOC and N-BVOC emissions on the OFP are further estimated and displayed in Figure 3b. Among all of the BVOC species, isoprene exhibits the largest OFPs, which is followed by methanol and other species (left three bars in Supporting Information Figure 5). The correlation between the U-BVOC OFPs and ratios of U-BVOC to N-BVOC emissions shown in Figure 3b implies a statistically significant ($P < 0.05$) positive relationship ($r = 0.54$; log−log scale). The areas with larger urban areas that correspond to higher ratios of U-BVOC to N-BVOC emissions (x-axis in Figure 3b) generally yield higher U-BVOC OFPs, particularly for those areas with urban fractions larger than 60% (yellow to red colors in Figure 3b), which tend to further demonstrate the critical role of considering the U-BVOC emissions when tackling air pollution issues in megacities.

3.3. Interannual Variations of U-BVOC Emissions Modulated by the Meteorology. In addition to discussing the mean values, the inter-annual variations in U-BVOC emissions (gray in Figure 4), as well as the observed maximum daily 8-h (MDA8) ozone levels (blue in Figure 4; http://www.pm25.in, last access: 10 July 2021) from 2015 to 2019 in China and the selected region of the NCP that is prone to ozone pollution occurrences[36,53] are shown in Figure 4. It should be noted that the five-year U-BVOC emissions generated from MEGAN reflect the sole modulation by meteorology since all other factors were the same as 2017. There are clear variations in the U-BVOC emissions, with the latter 3 years from 2017 to 2019 having substantially higher emissions than the first two years from 2015 to 2016, from either the annual (left of Figure 4) or seasonal perspective over summer (right of Figure 4) across of the entire China (top of Figure 4) or the selected region over the NCP (bottom of Figure 4), and the coverage of the NCP was the same as that in the top green square in Figure 1. This trend that is reflected in the U-BVOC emissions (grey in Figure 4) agrees well with the variations in MDA8 ozone levels. There are increases of 2.25 ppbv annually and 2.71 ppbv per summer in MDA8 ozone concentration in China, and the increases are much higher in the NCP, with 3.80 ppbv on the annual scale and 5.32 ppbv in summer. Moreover, the continuous increases lead to the MDA8 ozone levels exceeding the Class II level (82 ppbv) in the Technical Regulation on Ambient Air Quality Index (HJ633-2012) even when averaged over the entire NCP in 2019 (dashed blue line in Figure 4d). The correlations between the U-BVOC emissions and MDA8 ozone levels are highest in summer, which are implicative of the potentially strong connection between U-BVOCs and MDA8 ozone. The U-BVOC emissions might be highly efficient in triggering ozone formation, and this enhancement may be even higher than that from N-BVOC emissions.[25]

Considering that BVOC emissions are strongly driven by meteorological factors such as temperature, we also investigated the effect of heat waves, which are often concomitant with high temperatures and strong radiation levels,[15] in modulating the U-BVOC emissions. For each grid, heat wave events are defined as three consecutive days of daily maximum 2 m temperatures that are above a certain threshold (e.g., 95th percentile in this study) in the five-year period from 2015 to 2019.[54−57] Regional heat wave events are further defined when more than half of the grids in a particular region simultaneously experience heat waves. Three regions of the NCP, YRD, and PRD (the green squares in Figure 1) are selected to investigate the effect of heat waves on BVOC emissions (Figure 5), with total numbers of regional heat wave

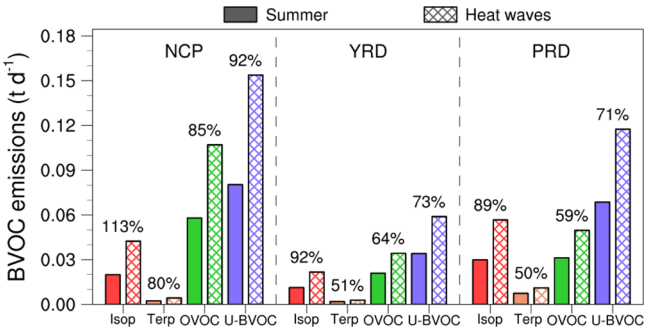

Figure 5. Emissions of isoprene (Isop), terpenes (Terp), OVOCs, and U-BVOCs over the NCP, YRD, and PRD during summer (solid bars) and regional heat wave periods (hatched bars) during 2015−2019. All emissions reported here are scaled to daily total basis. The percentages at the tops of the hatched bars represent the emission increases (%) during the regional heat waves compared to the summer average.

days of 19, 42, and 14 days, respectively, during 2015−2019. Triggered by the heat waves, the estimated U-BVOC emissions increase substantially in all three regions, with the largest increase of 92% in U-BVOC emissions over the NCP and an even higher increase (113%) in the isoprene emissions. As was discussed in Curci et al.,[58] the increase in BVOC emissions may have triggered a doubling of the BVOC-induced ozone concentrations in Paris during the scorching heat wave period in 2003, which is indicative of a potentially large effect on BVOCs and, in particular U-BVOCs, during recent heat waves.

3.4. High-Resolution U-BVOC and N-BVOC Emission Inventory at 1 km. To further examine the U-BVOCs at the city level, the U-BVOC emissions at a high spatial resolution of 1 km inside the NCP, YRD, and PRD (the simulation domains are shown in red squares in Figure 1) are displayed in Figure 6.

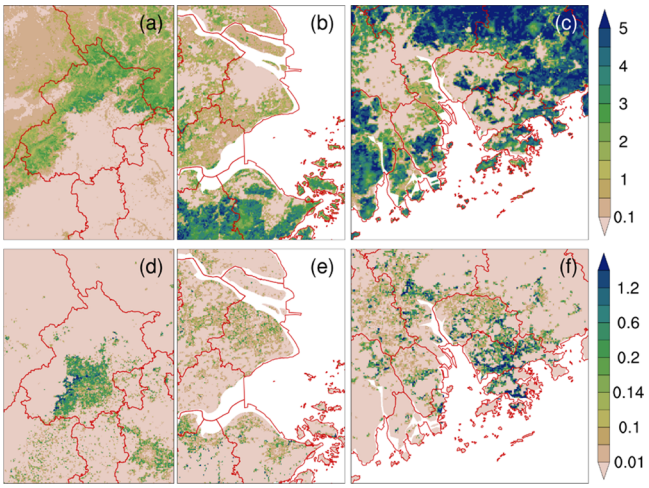

Figure 6. Spatial distributions of N-BVOC (a−c) and U-BVOC (d−f) emissions at 1 km spatial resolutions (red boxes in Figure 1) inside the NCP, YRD, and PRD during summer 2017 (t km^{-2} mon^{-1}).

The N-BVOC emission estimates based on MODIS data (top row) show that the rural areas of nearly all of the three developed regions are fully filled with BVOC emissions due to the large amounts of forest, while negligible amounts of BVOC emissions are located in the core urban areas (also explained in Section 2.3). The U-BVOC emissions shown in the bottom row (based on the FROM-GLC10 data) clearly delineate the

https://doi.org/10.1021/acs.est.1c06170
Environ. Sci. Technol. 2022, 56, 175−184

BVOC distributions over the urban cores and emphasize the importance of considering these emissions. There are large spatially heterogeneous urban landscapes even within cities, for example, the existence of large gradients in Beijing. Considering that the lifetime of isoprene, which is one of the most reactive VOCs, is relatively short (e.g., 20 min in urban Beijing according to Bryant et al.[59]), the large spatial heterogeneity may trigger larger differences in the ozone formation rates across the city and, in particular, when heat waves that are concomitant with stagnant weather are unfavorable for dispersion.[56,60]

3.5. Uncertainties and Limitations in the U-BVOC Calculations. In this study, the U-BVOC emission inventory is developed based on land cover data at a spatial resolution of 10 m. There are some limitations.

First, it is acknowledged that the 10 m data set is very large and requires substantial efforts to process. Nevertheless, the results in this study indicate that the number of urban trees may still be underestimated at this spatial resolution when considering the scattered nature of urban greenery as well as the comparisons with previous studies that were based on urban vegetation surveys in megacities like Beijing,[23] as discussed in Section 3.2. It emphasizes that even higher spatial resolution land cover data are preferred to further improve the identification of urban trees and subsequently the estimations of U-BVOC emissions.

Second, the emission rates of urban plants from urban green spaces may become higher than the values used in the look-up table, and the potentially higher emissions rates are primarily due to the higher intensities of heat waves, droughts, ozone exposures, and other stress factors.[61,62] For example, higher temperatures in urban areas when compared to the natural environment are common due to the urban heat island effect which promotes higher U-BVOC emissions via direct meteorological effects,[63] and there is also greater biomass due to altered growing conditions.[20] Based on laboratory studies, Ghirardo et al.[61] discovered that ozone exposure caused plants in urban Beijing to emit emissions due to extra stress, which accounts for a large fraction of the unstressed BVOC emissions. Moreover, the effect of drought on isoprene emissions is not considered in MEGANv2.1, while the newly released MEGAN version 3.0 (MEGANv3.0) incorporates the dipole effects of photosynthesis and water stress on isoprene emissions during drought, with enhanced emissions during the short-term and mild drought but decreased emissions during severe drought.[64−66]

Third, the vegetation types in urban areas are often different from those in rural areas, which may result in different emission factors, which may shift the seasonal emission patterns in urban areas in comparison to rural areas where the BVOCs tend to be primarily emitted in summer. For instance, based on the observations in 2009 in Boulder, Colorado, Baghi et al.[67] found substantial increases in BVOC emissions in spring over the urban area due to the blooming of ornamental flowering plants although they noted that the floral emissions provided only 11% of the total terpenes flux. Niinemets and Peñuelas[19] also indicated that winter emissions might increase due to the planting of evergreens in cool-temperate and temperate urban green spaces.

4. DISCUSSION

Based upon 10 m spatial resolution land cover data, we developed the first estimates at high spatial resolutions from 27 to 1 km of the BVOC emissions from urban green spaces throughout China. The regions with the largest U-BVOC emissions are co-located with the developed areas in China, which included the NCP, YRD, and PRD. Considering the previous lack of information regarding U-BVOC emissions, we expect that these data may bridge this gap and potentially play pivotal roles in elucidating the underestimation issues of simulated ozone concentration that have commonly been reported particularly during high ozone episodes.[27−29] The new U-BVOC emissions can modulate the atmospheric chemistry and thereby affect the formation of ozone and SOA. Meanwhile, considering the uncertainty in the U-BVOCs, we therefore call for a joint effort to develop even more accurate land cover data or to develop a hybrid method by combining satellite data and statistics to continue to improve U-BVOC emission inventories and reveal the critical role of U-BVOCs in affecting the urban chemistry.

BVOC emission models such as MEGAN are widely used all around the world, and the current emission inventory only focuses on China. Nevertheless, the concept proposed in this study is applicable to the entire world. Thus, future work in assessing the U-BVOC emissions over the world is essential for understanding their influence on the atmospheric chemistry across the globe. Meanwhile, many countries have initiated a mission of carbon neutrality, and China recently announced a challenging target that aims to achieve carbon neutrality by 2060. All of these goals may present a substantial need to increase the carbon sink, which may inevitably stimulate increased green spaces. Therefore, the U-BVOC emissions with a potential of increase may play an even more important role under an irreversible trend of decreasing anthropogenic emissions. Accurate estimations of U-BVOC emissions and their potential interactions with anthropogenic emissions may become a key process to fully elucidate their modulation on the atmospheric chemistry in China[5] and the entire globe.

■ ASSOCIATED CONTENT

Supporting Information

The Supporting Information is available free of charge at https://pubs.acs.org/doi/10.1021/acs.est.1c06170.

Comparison between observed and simulated meteorological parameters; 16 types of PFTs in MEGAN; types of land cover in the MODIS MCD12Q1 data; types of land cover in the FROM-GLC10 data; Input datasets for MEGAN; provincial mean annual U-BVOC and N-BVOC emissions; spatial distributions of annual isoprene, terpenes, OVOC, and T-BVOC emissions; spatial distribution of the fraction of four major PFTs; spatial distributions of the land cover data; spatial distributions of the ratio of provincial annual U-BVOC to N-BVOC emissions; and annual OFPs of N-BVOC and U-BVOC emissions of each BVOC species (PDF)

■ AUTHOR INFORMATION

Corresponding Author

Yang Gao − *Frontiers Science Center for Deep Ocean Multispheres and Earth System, and Key Laboratory of Marine Environment and Ecology, Ministry of Education, Ocean University of China, and Qingdao National Laboratory for Marine Science and Technology, Qingdao 266100, China;* orcid.org/0000-0001-6444-6544; Email: yanggao@ouc.edu.cn

https://doi.org/10.1021/acs.est.1c06170
Environ. Sci. Technol. 2022, 56, 175−184

Authors

Mingchen Ma − *Frontiers Science Center for Deep Ocean Multispheres and Earth System, and Key Laboratory of Marine Environment and Ecology, Ministry of Education, Ocean University of China, and Qingdao National Laboratory for Marine Science and Technology, Qingdao 266100, China*

Aijun Ding − *Joint International Research Laboratory of Atmospheric and Earth System Sciences, School of Atmospheric Sciences, Nanjing University, Nanjing 210023, China*

Hang Su − *Multiphase Chemistry Department, Max Planck Institute for Chemistry, Mainz D 55128, Germany; State Environmental Protection Key Laboratory of Formation and Prevention of Urban Air Pollution Complex, Shanghai Academy of Environmental Sciences, Shanghai 200233, China;* orcid.org/0000-0003-4889-1669

Hong Liao − *Jiangsu Key Laboratory of Atmospheric Environment Monitoring and Pollution Control, Jiangsu Engineering Technology Research Center of Environmental Cleaning Materials, Collaborative Innovation Center of Atmospheric Environment and Equipment Technology, School of Environmental Science and Engineering, Nanjing University of Information Science and Technology, Nanjing 210044, China*

Shuxiao Wang − *State Key Joint Laboratory of Environment Simulation and Pollution Control, School of Environment, Tsinghua University, Beijing 100084, China;* orcid.org/0000-0001-9727-1963

Xuemei Wang − *Institute for Environmental and Climate Research, Jinan University, Guangzhou 510000, China*

Bin Zhao − *State Key Joint Laboratory of Environment Simulation and Pollution Control, School of Environment, Tsinghua University, Beijing 100084, China;* orcid.org/0000-0001-8438-9188

Shaoqing Zhang − *Laboratory for Ocean Dynamics and Climate, Qingdao National Laboratory for Marine Science and Technology, Qingdao 266237, China; International Laboratory for High-Resolution Earth System Model and Prediction (iHESP), Qingdao 266100, China; Key Laboratory of Physical Oceanography, Institute for Advanced Ocean Study, Frontiers Science Center for Deep Ocean Multispheres and Earth System (FDOMES), College of Oceanic and Atmospheric Sciences, Ocean University of China, Qingdao 266100, China*

Pingqing Fu − *Institute of Surface-Earth System Science, Tianjin University, Tianjin 300072, China;* orcid.org/0000-0001-6249-2280

Alex B. Guenther − *Department of Earth System Science, University of California Irvine, Irvine, California 92697, United States*

Minghuai Wang − *Joint International Research Laboratory of Atmospheric and Earth System Sciences, School of Atmospheric Sciences, Nanjing University, Nanjing 210023, China*

Shenshen Li − *State Key Laboratory of Remote Sensing Science, Aerospace Information Research Institute, Chinese Academy of Sciences, Beijing 100101, China*

Biwu Chu − *State Key Joint Laboratory of Environment Simulation and Pollution Control, Research Center for Eco-Environmental Sciences, Chinese Academy of Sciences, Beijing 100085, China;* orcid.org/0000-0002-7548-5669

Xiaohong Yao − *Frontiers Science Center for Deep Ocean Multispheres and Earth System, and Key Laboratory of Marine Environment and Ecology, Ministry of Education, Ocean University of China, and Qingdao National Laboratory for Marine Science and Technology, Qingdao 266100, China;* orcid.org/0000-0002-2960-0793

Huiwang Gao − *Frontiers Science Center for Deep Ocean Multispheres and Earth System, and Key Laboratory of Marine Environment and Ecology, Ministry of Education, Ocean University of China, and Qingdao National Laboratory for Marine Science and Technology, Qingdao 266100, China*

Complete contact information is available at: https://pubs.acs.org/10.1021/acs.est.1c06170

Notes

The authors declare no competing financial interest.

■ ACKNOWLEDGMENTS

This research was supported by grants from the National Natural Science Foundation of China (91744208, 42122039, and 21625701) and Special Fund Project for Science and Technology Innovation Strategy of Guangdong Province (Grant No. 2019B121205004). The analysis was performed using the computing resources of Center for High Performance Computing and System Simulation, Pilot National Laboratory for Marine Science and Technology (Qingdao).

■ REFERENCES

(1) Goldstein, A. H.; Galbally, I. E. Known and unexplored organic constituents in the earth's atmosphere. *Environ. Sci. Technol.* **2007**, *41*, 1514−1521.

(2) Guenther, A.; Hewitt, C. N.; Erickson, D.; Fall, R.; Geron, C.; Graedel, T.; Harley, P.; Klinger, L.; Lerdau, M.; Mckay, W. A.; Pierce, T.; Scholes, B.; Steinbrecher, R.; Tallamraju, R.; Taylor, J.; Zimmerman, P. A Global-Model of Natural Volatile Organic-Compound Emissions. *J. Geophys. Res.: Atmos.* **1995**, *100*, 8873−8892.

(3) Folberth, G. A.; Hauglustaine, D. A.; Lathière, J.; Brocheton, F. Interactive chemistry in the Laboratoire de Meteorologie Dynamique general circulation model: model description and impact analysis of biogenic hydrocarbons on tropospheric chemistry. *Atmos. Chem. Phys.* **2006**, *6*, 2273−2319.

(4) Monks, P. S.; Archibald, A. T.; Colette, A.; Cooper, O.; Coyle, M.; Derwent, R.; Fowler, D.; Granier, C.; Law, K. S.; Mills, G. E.; Stevenson, D. S.; Tarasova, O.; Thouret, V.; von Schneidemesser, E.; Sommariva, R.; Wild, O.; Williams, M. L. Tropospheric ozone and its precursors from the urban to the global scale from air quality to short-lived climate forcer. *Atmos. Chem. Phys.* **2015**, *15*, 8889−8973.

(5) Gao, Y.; Yan, F.; Ma, M.; Ding, A.; Liao, H.; Wang, S.; Wang, X.; Zhao, B.; Cai, W.; Su, H.; Yao, X.; Gao, H. Unveiling the dipole synergic effect of biogenic and anthropogenic emissions on ozone concentrations. *Sci. Total Environ.* **2021**, 151722.

(6) Yang, X.; Wu, K.; Wang, H.; Liu, Y.; Gu, S.; Lu, Y.; Zhang, X.; Hu, Y.; Ou, Y.; Wang, S.; Wang, Z. Summertime ozone pollution in Sichuan Basin, China: Meteorological conditions, sources and process analysis. *Atmos. Environ.* **2020**, *226*, 117392.

(7) Andreae, M. O.; Crutzen, P. J. Atmospheric aerosols: Biogeochemical sources and role in atmospheric chemistry. *Science* **1997**, *276*, 1052−1058.

(8) Ng, N. L.; Brown, S. S.; Archibald, A. T.; Atlas, E.; Cohen, R. C.; Crowley, J. N.; Day, D. A.; Donahue, N. M.; Fry, J. L.; Fuchs, H.; Griffin, R. J.; Guzman, M. I.; Herrmann, H.; Hodzic, A.; Iinuma, Y.; Jimenez, J. L.; Kiendler-Scharr, A.; Lee, B. H.; Luecken, D. J.; Mao, J.; McLaren, R.; Mutzel, A.; Osthoff, H. D.; Ouyang, B.; Picquet-Varrault, B.; Platt, U.; Pye, H. O. T.; Rudich, Y.; Schwantes, R. H.;

Shiraiwa, M.; Stutz, J.; Thornton, J. A.; Tilgner, A.; Williams, B. J.; Zaveri, R. A. Nitrate radicals and biogenic volatile organic compounds: oxidation, mechanisms, and organic aerosol. *Atmos. Chem. Phys.* **2017**, *17*, 2103−2162.
(9) Holopainen, J. K.; Kivimäenpää, M.; Nizkorodov, S. A. Plant-derived Secondary Organic Material in the Air and Ecosystems. *Trends Plant Sci.* **2017**, *22*, 744−753.
(10) Guenther, A.; Karl, T.; Harley, P.; Wiedinmyer, C.; Palmer, P. I.; Geron, C. Estimates of global terrestrial isoprene emissions using MEGAN (Model of Emissions of Gases and Aerosols from Nature). *Atmos. Chem. Phys.* **2006**, *6*, 3181−3210.
(11) Lun, X.; Lin, Y.; Chai, F.; Fan, C.; Li, H.; Liu, J. Reviews of emission of biogenic volatile organic compounds (BVOCs) in Asia. *J. Environ. Sci.* **2020**, *95*, 266−277.
(12) Churkina, G.; Kuik, F.; Bonn, B.; Lauer, A.; Grote, R.; Tomiak, K.; Butler, T. M. Effect of VOC Emissions from Vegetation on Air Quality in Berlin during a Heatwave. *Environ. Sci. Technol.* **2017**, *51*, 6120−6130.
(13) Yang, X.; Wu, K.; Lu, Y.; Wang, S.; Qiao, Y.; Zhang, X.; Wang, Y.; Wang, H.; Liu, Z.; Liu, Y.; Lei, Y. Origin of regional springtime ozone episodes in the Sichuan Basin, China: Role of synoptic forcing and regional transport. *Environ. Pollut.* **2021**, *278*, 116845.
(14) Wang, P.; Schade, G.; Estes, M.; Ying, Q. Improved MEGAN predictions of biogenic isoprene in the contiguous United States. *Atmos. Environ.* **2017**, *148*, 337−351.
(15) Ma, M.; Gao, Y.; Wang, Y.; Zhang, S.; Leung, L. R.; Liu, C.; Wang, S.; Zhao, B.; Chang, X.; Su, H.; Zhang, T.; Sheng, L.; Yao, X.; Gao, H. Substantial ozone enhancement over the North China Plain from increased biogenic emissions due to heat waves and land cover in summer 2017. *Atmos. Chem. Phys.* **2019**, *19*, 12195−12207.
(16) Friedl, M.; Sulla-Menashe, D. MCD12Q1 MODIS/Terra +Aqua Land Cover Type Yearly L3 Global 500m SIN Grid V006. In *NASA EOSDIS Land Processes DAAC*, 2019.
(17) Oke, T. R. *Applied Climatology: Principles and Practices*; Routledge: London, 1997; pp 273−287.
(18) Zhou, D.; Zhao, S.; Zhang, L.; Sun, G.; Liu, Y. The footprint of urban heat island effect in China. *Sci. Rep.* **2015**, *5*, 11160.
(19) Niinemets, Ü.; Peñuelas, J. Gardening and urban landscaping: significant players in global change. *Trends Plant Sci.* **2008**, *13*, 60−65.
(20) Gregg, J. W.; Jones, C. G.; Dawson, T. E. Urbanization effects on tree growth in the vicinity of New York City. *Nature* **2003**, *424*, 183−187.
(21) Simon, H.; Fallmann, J.; Kropp, T.; Tost, H.; Bruse, M. Urban Trees and Their Impact on Local Ozone Concentration-A Micro-climate Modeling Study. *Atmosphere* **2019**, *10*, 154.
(22) Chang, J.; Ren, Y.; Shi, Y.; Zhu, Y.; Ge, Y.; Hong, S.; Jiao, L.; Lin, F.; Peng, C.; Mochizuki, T.; Tani, A.; Mu, Y.; Fu, C. An inventory of biogenic volatile organic compounds for a subtropical urban−rural complex. *Atmos. Environ.* **2012**, *56*, 115−123.
(23) Ren, Y.; Qu, Z.; Du, Y.; Xu, R.; Ma, D.; Yang, G.; Shi, Y.; Fan, X.; Tani, A.; Guo, P.; Ge, Y.; Chang, J. Air quality and health effects of biogenic volatile organic compounds emissions from urban green spaces and the mitigation strategies. *Environ. Pollut.* **2017**, *230*, 849−861.
(24) Gu, S.; Guenther, A.; Faiola, C. Effects of Anthropogenic and Biogenic Volatile Organic Compounds on Los Angeles Air Quality. *Environ. Sci. Technol.* **2021**, *55*, 12191−12201.
(25) Gao, Y.; Ma, M. C.; Yan, F. F.; Su, H.; Wang, S. X.; Liao, H.; Zhao, B.; Wang, X. M.; Sun, Y. L.; Hopkins, J. R.; Chen, Q.; Fu, P. Q.; Lewis, A. C.; Qiu, Q. H.; Yao, X. H.; Gao, H. W. Impacts of biogenic emissions from urban landscapes on summer ozone and secondary organic aerosol formation in megacities. *Sci. Total Environ.* **2021**, 152654.
(26) Bell, M.; Ellis, H. Sensitivity analysis of tropospheric ozone to modified biogenic emissions for the Mid-Atlantic region. *Atmos. Environ.* **2004**, *38*, 1879−1889.
(27) Sun, J.; Shen, Z.; Wang, R.; Li, G.; Zhang, Y.; Zhang, B.; He, K.; Tang, Z.; Xu, H.; Qu, L.; Sai Hang Ho, S.; Liu, S.; Cao, J. A comprehensive study on ozone pollution in a megacity in North China Plain during summertime: Observations, source attributions and ozone sensitivity. *Environ. Int.* **2021**, *146*, 106279.
(28) Wang, R.; Tie, X.; Li, G.; Zhao, S.; Long, X.; Johansson, L.; An, Z. Effect of ship emissions on O3 in the Yangtze River Delta region of China: Analysis of WRF-Chem modeling. *Sci. Total Environ.* **2019**, *683*, 360−370.
(29) Lu, X.; Zhang, S.; Xing, J.; Wang, Y.; Chen, W.; Ding, D.; Wu, Y.; Wang, S.; Duan, L.; Hao, J. Progress of Air Pollution Control in China and Its Challenges and Opportunities in the Ecological Civilization Era. *Engineering* **2020**, *6*, 1423−1431.
(30) Gong, P.; Li, X. C.; Wang, J.; Bai, Y. Q.; Cheng, B.; Hu, T. Y.; Liu, X. P.; Xu, B.; Yang, J.; Zhang, W.; Zhou, Y. Y. Annual maps of global artificial impervious area (GAIA) between 1985 and 2018. *Remote Sens. Environ.* **2020**, *236*, 111510.
(31) Zhao, J.; Chen, S.; Jiang, B.; Ren, Y.; Wang, H.; Vause, J.; Yu, H. Temporal trend of green space coverage in China and its relationship with urbanization over the last two decades. *Sci. Total Environ.* **2013**, *442*, 455−465.
(32) Kuang, W.; Zhang, S.; Li, X.; Lu, D. A 30 m resolution dataset of China's urban impervious surface area and green space, 2000-2018. *Earth Syst. Sci. Data* **2021**, *13*, 63−82.
(33) Gong, P.; Liu, H.; Zhang, M.; Li, C.; Wang, J.; Huang, H.; Clinton, N.; Ji, L.; Li, W.; Bai, Y.; Chen, B.; Xu, B.; Zhu, Z.; Yuan, C.; Ping Suen, H.; Guo, J.; Xu, N.; Li, W.; Zhao, Y.; Yang, J.; Yu, C.; Wang, X.; Fu, H.; Yu, L.; Dronova, I.; Hui, F.; Cheng, X.; Shi, X.; Xiao, F.; Liu, Q.; Song, L. Stable classification with limited sample: transferring a 30-m resolution sample set collected in 2015 to mapping 10-m resolution global land cover in 2017. *Sci. Bull.* **2019**, *64*, 370−373.
(34) Guenther, A. B.; Jiang, X.; Heald, C. L.; Sakulyanontvittaya, T.; Duhl, T.; Emmons, L. K.; Wang, X. The Model of Emissions of Gases and Aerosols from Nature version 2.1 (MEGAN2.1): an extended and updated framework for modeling biogenic emissions. *Geosci. Model Dev.* **2012**, *5*, 1471−1492.
(35) Gao, Y.; Leung, L. R.; Zhao, C.; Hagos, S. Sensitivity of US summer precipitation to model resolution and convective parameterizations across gray zone resolutions. *J. Geophys. Res.: Atmos.* **2017**, *122*, 2714−2733.
(36) Yan, F.; Gao, Y.; Ma, M.; Liu, C.; Ji, X.; Zhao, F.; Yao, X.; Gao, H. Revealing the modulation of boundary conditions and governing processes on ozone formation over northern China in June 2017. *Environ. Pollut.* **2021**, *272*, 115999.
(37) Zhang, G.; Gao, Y.; Cai, W.; Leung, L. R.; Wang, S.; Zhao, B.; Wang, M.; Shan, H.; Yao, X.; Gao, H. Seesaw haze pollution in North China modulated by the sub-seasonal variability of atmospheric circulation. *Atmos. Chem. Phys.* **2019**, *19*, 565−576.
(38) Gao, Y.; Shan, H. Y.; Zhang, S. Q.; Sheng, L. F.; Li, J. P.; Zhang, J. X.; Ma, M. C.; Meng, H.; Luo, K.; Gao, H. W.; Yao, X. H. Characteristics and sources of PM2.5 with focus on two severe pollution events in a coastal city of Qingdao, China. *Chemosphere* **2020**, *247*, 125861.
(39) Giorgi, F.; Shields Brodeur, C.; Bates, G. T. Regional climate change scenarios over the United States produced with a nested regional climate model. *J. Clim.* **1994**, *7*, 375−399.
(40) Stauffer, D. R.; Seaman, N. L. Use of Four-Dimensional Data Assimilation in a Limited-Area Mesoscale Model. Part I: Experiments with Synoptic-Scale Data. *Mon. Weather Rev.* **1990**, *118*, 1250−1277.
(41) Saha, S.; Moorthi, S.; Wu, X.; Wang, J.; Nadiga, S.; Tripp, P.; Behringer, D.; Hou, Y.-T.; Chuang, H.-y.; Iredell, M.; Ek, M.; Meng, J.; Yang, R.; Mendez, M. P.; Van Den Dool, H.; Zhang, Q.; Wang, W.; Chen, M.; Becker, E. The NCEP Climate Forecast System Version 2. *J. Clim.* **2014**, *27*, 2185−2208.
(42) Myneni, R.; Knyazikhin, Y.; Park, T. MODIS/Terra+Aqua Leaf Area Index/FPAR 8-Day L4 Global 500m SIN Grid V061. In *NASA EOSDIS Land Processes DAAC*, 2021.
(43) Zhang, P.; Anderson, B.; Barlow, M. Climate-related vegetation characteristics derived from Moderate Resolution Imaging Spectroradiometer (MODIS) leaf area index and normalized difference vegetation index. *J. Geophys. Res.: Atmos.* **2004**, *109*, 1−13.

https://doi.org/10.1021/acs.est.1c06170
Environ. Sci. Technol. 2022, 56, 175−184

(44) Carter, W. *Development of the Saprc-07 Chemical Mechanism and Updated Ozone Reactivity Scales*; Center for Environmental Research and Technology, University of California: Riverside, CA, 2010.
(45) Wu, K.; Yang, X.; Chen, D.; Gu, S.; Lu, Y.; Jiang, Q.; Wang, K.; Ou, Y.; Qian, Y.; Shao, P.; Lu, S. Estimation of biogenic VOC emissions and their corresponding impact on ozone and secondary organic aerosol formation in China. *Atmos. Res.* **2020**, *231*, 104656.
(46) Klinger, L. F.; Li, Q. J.; Guenther, A. B.; Greenberg, J. P.; Baker, B.; Bai, J. H. Assessment of volatile organic compound emissions from ecosystems of China. *J. Geophys. Res.: Atmos.* **2002**, *107*, 4603.
(47) Chi, Y. Q.; Xie, S. Spatiotemporal Inventory of Biogenic Volatile Organic Compound Emissions in China Based on Vegetation Volume and Production. *Acta Sci. Nat. Univ. Pekin.* **2012**, *48*, 475−482.
(48) Li, L. Y.; Chen, Y.; Xie, S. D. Spatio-temporal variation of biogenic volatile organic compounds emissions in China. *Environ. Pollut.* **2013**, *182*, 157−168.
(49) Ou, J.; Yuan, Z.; Zheng, J.; Huang, Z.; Shao, M.; Li, Z.; Huang, X.; Guo, H.; Louie, P. K. K. Ambient Ozone Control in a Photochemically Active Region: Short Term Despiking or Long-Term Attainment? *Environ. Sci. Technol.* **2016**, *50*, 5720−5728.
(50) Yang, W.; Chen, H.; Wang, W.; Wu, J.; Li, J.; Wang, Z.; Zheng, J.; Chen, D. Modeling study of ozone source apportionment over the Pearl River Delta in 2015. *Environ. Pollut.* **2019**, *253*, 393−402.
(51) Wang, Z.; Li, Y.; Chen, T.; Zhang, D.; Sun, F.; Wei, Q.; Dong, X.; Sun, R.; Huan, N.; Pan, L. Ground-level ozone in urban Beijing over a 1-year period: Temporal variations and relationship to atmospheric oxidation. *Atmos. Res.* **2015**, *164−165*, 110−117.
(52) Shao, M.; Wang, W.; Yuan, B.; Parrish, D. D.; Li, X.; Lu, K.; Wu, L.; Wang, X.; Mo, Z.; Yang, S.; Peng, Y.; Kuang, Y.; Chen, W.; Hu, M.; Zeng, L.; Su, H.; Cheng, Y.; Zheng, J.; Zhang, Y. Quantifying the role of PM2.5 dropping in variations of ground-level ozone: Inter-comparison between Beijing and Los Angeles. *Sci. Total Environ.* **2021**, *788*, 147712.
(53) Li, K.; Jacob, D. J.; Liao, H.; Shen, L.; Zhang, Q.; Bates, K. H. Anthropogenic drivers of 2013-2017 trends in summer surface ozone in China. *Proc. Natl. Acad. Sci. U.S.A.* **2018**, *116*, 422−427.
(54) Gao, Y.; Fu, J. S.; Drake, J. B.; Liu, Y.; Lamarque, J.-F. Projected changes of extreme weather events in the eastern United States based on a high resolution climate modeling system. *Environ. Res. Lett.* **2012**, *7*, 044025.
(55) Gao, Y.; Fu, J. S.; Drake, J. B.; Lamarque, J.-F.; Liu, Y. The impact of emission and climate change on ozone in the United States under representative concentration pathways (RCPs). *Atmos. Chem. Phys.* **2013**, *13*, 9607−9621.
(56) Zhang, J.; Gao, Y.; Luo, K.; Leung, L. R.; Zhang, Y.; Wang, K.; Fan, J. Impacts of compound extreme weather events on ozone in the present and future. *Atmos. Chem. Phys.* **2018**, *18*, 9861−9877.
(57) Sillmann, J.; Kharin, V. V.; Zhang, X.; Zwiers, F. W.; Bronaugh, D. Climate extremes indices in the CMIP5 multimodel ensemble: Part 1. Model evaluation in the present climate. *J. Geophys. Res.: Atmos.* **2013**, *118*, 1716−1733.
(58) Curci, G.; Beekmann, M.; Vautard, R.; Smiatek, G.; Steinbrecher, R.; Theloke, J.; Friedrich, R. Modelling study of the impact of isoprene and terpene biogenic emissions on European ozone levels. *Atmos. Environ.* **2009**, *43*, 1444−1455.
(59) Bryant, D. J.; Dixon, W. J.; Hopkins, J. R.; Dunmore, R. E.; Pereira, K. L.; Shaw, M.; Squires, F. A.; Bannan, T. J.; Mehra, A.; Worrall, S. D.; Bacak, A.; Coe, H.; Percival, C. J.; Whalley, L. K.; Heard, D. E.; Slater, E. J.; Ouyang, B.; Cui, T.; Surratt, J. D.; Liu, D.; Shi, Z.; Harrison, R.; Sun, Y.; Xu, W.; Lewis, A. C.; Lee, J. D.; Rickard, A. R.; Hamilton, J. F. Strong anthropogenic control of secondary organic aerosol formation from isoprene in Beijing. *Atmos. Chem. Phys.* **2020**, *20*, 7531−7552.
(60) Gao, Y.; Zhang, J.; Yan, F.; Leung, L. R.; Luo, K.; Zhang, Y.; Bell, M. L. Nonlinear effect of compound extreme weather events on ozone formation over the United States. *Weather. Clim. Extremes* **2020**, *30*, 100285.
(61) Ghirardo, A.; Xie, J.; Zheng, X.; Wang, Y.; Grote, R.; Block, K.; Wildt, J.; Mentel, T.; Kiendler-Scharr, A.; Hallquist, M.; Butterbach-Bahl, K.; Schnitzler, J.-P. Urban stress-induced biogenic VOC emissions and SOA-forming potentials in Beijing. *Atmos. Chem. Phys.* **2016**, *16*, 2901−2920.
(62) Calfapietra, C.; Fares, S.; Manes, F.; Morani, A.; Sgrigna, G.; Loreto, F. Role of Biogenic Volatile Organic Compounds (BVOC) emitted by urban trees on ozone concentration in cities: A review. *Environ. Pollut.* **2013**, *183*, 71−80.
(63) Niinemets, Ü.; Monson, R. K.; Arneth, A.; Ciccioli, P.; Kesselmeier, J.; Kuhn, U.; Noe, S. M.; Peñuelas, J.; Staudt, M. The leaf-level emission factor of volatile isoprenoids: caveats, model algorithms, response shapes and scaling. *Biogeosciences* **2010**, *7*, 1809−1832.
(64) Pegoraro, E.; Rey, A.; Greenberg, J.; Harley, P.; Grace, J.; Malhi, Y.; Guenther, A. Effect of drought on isoprene emission rates from leaves of Quercus virginiana Mill. *Atmos. Environ.* **2004**, *38*, 6149−6156.
(65) Jiang, X.; Guenther, A.; Potosnak, M.; Geron, C.; Seco, R.; Karl, T.; Kim, S.; Gu, L.; Pallardy, S. Isoprene emission response to drought and the impact on global atmospheric chemistry. *Atmos. Environ.* **2018**, *183*, 69−83.
(66) Wang, Y.; Tan, X.; Huang, L.; Wang, Q.; Li, H.; Zhang, H.; Zhang, K.; Liu, Z.; Traore, D.; Yaluk, E.; Fu, J. S.; Li, L. The impact of biogenic emissions on ozone formation in the Yangtze River Delta region based on MEGANv3.1. *Air Qual., Atmos. Health* **2021**, *14*, 763−774.
(67) Baghi, R.; Helmig, D.; Guenther, A.; Duhl, T.; Daly, R. Contribution of flowering trees to urban atmospheric biogenic volatile organic compound emissions. *Biogeosciences* **2012**, *9*, 3777−3785.

https://doi.org/10.1021/acs.est.1c06170
Environ. Sci. Technol. 2022, 56, 175−184